

Dumitru I. Caruntu¹

Mem ASME

Department of Mechanical Engineering,
University of Texas Rio Grande Valley,
1201 W University Drive,
Edinburg, TX 78539
e-mails: dumitru.caruntu@utrgv.edu;
caruntud2@asme.org

Ricardo Moreno

Department of Mechanical Engineering,
University of Texas Rio Grande Valley,
1201 W University Drive,
Edinburg, TX 78539
e-mail: rmoreno851@gmail.com

Human Knee Inverse Dynamics Model of Vertical Jump Exercise

This work deals with the dynamics of the human knee during vertical jump exercise. The focus is on the joint forces necessary to produce the jump and to dissipate energy during landing. A two-dimensional (2D) sagittal plane, inverse dynamics human leg model is developed. This model uses data from a motion capture system and force plates in order to predict knee and hip joint forces during the vertical jump exercise. The model consists of three bony structures femur, tibia, and patella, ligament structures to include both cruciate and collateral ligaments, and knee joint muscles. The inverse dynamics model is solved using optimization in order to predict joint forces during this exercise. MATLAB software package is used for the optimization computations. Results are compared with data available in the literature. This work provides insight regarding contact forces and ligaments forces, muscle forces, and knee and hip contact forces in the vertical jump exercise. [DOI: 10.1115/1.4044246]

1 Introduction

Biomechanics is an active field of research that gives insight in areas such as sports, ergonomics, and bioengineering. Biomechanics research may improve procedures in rehabilitation, product design, and work environments [1]. There have been many advances in computer modeling, data acquisition, motion simulations, and image rendering with biomechanical data. Biomechanical data have been used to replicate movements in robots and make their motion more lifelike with the “ability to perform fast movements, other properties, and particularities” [2]. In biomechanics, models are built to investigate joint motion, and contact, ligament, and muscle forces during exercises such as walking and running.

Anatomical, biochemical, and physiological characteristics, all contribute to musculoskeletal system [3], which is continuously acting since the human body is an “inherently unstable system” [4]. Understanding the behavior of the musculoskeletal system gives perspective to daily life tasks. Few investigations have been dedicated to leg dynamics with faster execution speeds to include loads on the hip and knee joints [5]. Understanding these motions allows for more insight in the human potential, since sporting activities produce forces 3–4.5 times the person’s bodyweight [5]. These performance-based movements could be simplified to a simple jump and landing motion.

Vertical jump is a ballistic movement, which can be considered “one of the most ‘explosive’ tests due to both, its very short duration, and the high intensity involved” [6]. The vertical jump exercise can be broken down into four distinct phases: (1) standing position, (2) jumping, (3) flight time, and (4) landing. Landing, often described as deceleration and stabilization of the body after contact [7], is the essential part of injury prevention, which can vary given the situation. Joint kinematics and kinetics, energy absorption strategies, muscle activation patterns, and landing style are a few factors that influence landing mechanics [8]. Landing styles can vary from toe-heel, flatfoot, toe-only, and heel-only [9]. The overall goal in a landing strategy is to dissipate the force effectively produced by the contact [10].

Deterring from injury is the goal in executing a movement. The knee is the most commonly injured joint and with the most severity [9]. The most “catastrophic knee injuries that debilitate athletic

careers” are ligament ruptures [11] of which 70–80% occur in noncontact situations, without any external interference, person-to-person contact, or object-to-person contact [12]. From these noncontact situations, the rupture of the anterior cruciate ligament (ACL) could be attributed to landing [8]. Injuries of this nature are usually in one-legged landings and are “considered more dangerous because of the decreased base of support and the increased demand required by absorption of the impact of landing” [13]. However, injuries can happen during two-legged landings as well.

Understanding these mechanisms is beneficial for performance-based tasks or rehabilitation. Mathematical models are used to predict the characteristics of human movement. The equations of motion are used as equality constraints in inverse dynamics models. However, the difficulty lies in finding a “physiologically feasible set of controls” for the system [14]. In doing so, an objective function could be defined on the motor task [7].

Recent research reported in the literature and dedicated to vertical jump exercise includes strength and conditioning [15–17] and physiotherapy [18]. Hirayama [15] examined the acute effects of an ascending intensity squat protocol consisting of single-repetition exercises on subsequent vertical jump performance. Perez-Castilla et al. [16] compared the reliability and magnitude of jump height between the two standard procedures of analyzing force platform data to estimate jump height. Fukutani et al. [17] examined the influence of the intensity of squat exercises on the subsequent jump performance and the magnitude of the phenomenon of postactivation potentiation. Paul and Kumar [18] reported the effect of split jump and vertical jump exercise on dynamic balance and compared the effect of exercise on the dynamic balance among female netball players.

Investigations on vertical jump exercise have been reported by Cleather et al. [5], Spägle et al. [7], and Blajer et al. [19]. Specifically, Cleather et al. [5] used a biomechanical model of the right lower limb to calculate the internal joint forces experienced by the lower limb during vertical jumping with a particular emphasis on the forces experienced by the knee. They used an inverse dynamics approach in which the experimental data used were from twelve athletic males (age 27.1 ± 4.30 yr; mass 83.7 ± 9.90 kg) who performed five maximal countermovement jumps (CMJs) with their hands on their hips and the highest jump (height 0.38 ± 0.05 m). They reported the tibio-femoral joint and hip joint loadings experienced by a typical subject during vertical jumping and landing to be 6.50 times body weight (BW) and 3.70 BW, respectively. Spägle et al. [7] applied a multiphase dynamic optimization approach to a real human vertical one-legged jump consisting of an upward propulsion, an airborne and a landing phase. They aimed to understand how the central nervous system

¹Corresponding author.

Contributed by the Design Engineering Division of ASME for publication in the JOURNAL OF COMPUTATIONAL AND NONLINEAR DYNAMICS. Manuscript received September 27, 2018; final manuscript received June 27, 2019; published online September 12, 2019. Assoc. Editor: Elena G. Tolkacheva.

coordinates muscle excitations in order to accelerate and decelerate body segments of the lower limb for a measured one-legged, vertical jump. They reported the normalized muscle excitations of their nine muscles model of the lower limb. Biceps femoris long head and biceps femoris short head showed very little normalized muscle excitations. Blajer et al. [19] presented a two-dimensional (2D) biomechanical model of a human body for determination of the muscle forces and joint reaction forces in the lower extremities during sagittal plane movements such as vertical jump. The experimental results used in the model were from a vertical jump performed by an athlete (basketball player) of mass 114.8 kg and height 194 cm. While the hip, knee, and ankle joints were modeled as enforced directly by the muscle forces applied to the foot, shank, thigh, and pelvis at the muscle attachment points, the actuation of the other joints was simplified to the torques representing the respective muscle action. They reported a peak of the total force of the vasti muscles (medialis, lateralis, and intermedius) of 3.40 times body weight.

Present work investigates the muscular, ligament, and contact forces, and tibio-femoral contact point trajectory associated with vertical jump exercise, i.e., CMJ with the arms kept akimbo. The present vertical jump consists of larger jumping duration and similar landing duration when compared to the explosive vertical jump in Ref. [5]. To investigate internal forces experienced during the vertical jump exercise, a 2D human leg model was developed using a Newton–Euler formulation. Using an inverse dynamics approach, the mathematical model predicted the internal forces during the exercise. Although the vertical squat jump exercise has been previously investigated, it is not completely understood. To the best of our knowledge, the novelty of this work consists of reporting the significant forces experienced by the human leg during the vertical jump exercise, namely (1) tibio-femoral, patello-femoral, and hip contact forces; (2) gluteus, quadriceps, and gastrocnemius muscle forces; and (3) posterior cruciate ligament (PCL) and medial collateral ligament (MCL). Also, this work reports (4) the tibio-femoral contact point trajectory during the moderate vertical squat jump exercise. In this research, the human subject was a recreational athlete, an advent runner, familiar to consistent execution. The subject was 1.75 m tall and had a mass of 84 kg. The largest values reached during jumping and landing were: knee flexion angles 95.4 deg and 55.4 deg, vertical ground reaction force 1.10 times BW and 2.70 BW, quadriceps muscle 1.10 BW and 2.50 BW, gluteus muscle 2.10 BW and 1.12 BW, gastrocnemius muscle 1.40 BW and 2.80 BW, tibio-femoral joint contact 2.10 BW and 5.60 BW, patello-femoral contact 1.10 BW and 2.00 BW, and hip contact force 1.60 BW and 2.40 BW, PCL 0.55 BW and 0.65 BW, and MCL 0.22 BW and 1.10 BW, respectively.

Significant forces throughout the entire exercise were ground reaction forces (GRF), quadriceps and gluteus muscle forces, contact forces (tibio-femoral, patello-femoral, and hip), and PCL force. Except gluteus, all these forces reached a maximum during the ascent phase of the jumping. Forces that showed a maximum at the lowest jumping position of 95.4 deg flexion angle were quadriceps and gluteus muscle forces, PCL force, and tibio-femoral contact force. Forces that were significant only right before take-off and the first phase of landing were gastrocnemius muscle and MCL. Forces included in the model that showed no significant values were hamstrings and iliacus muscles, ACL, and lateral collateral ligament (LCL).

The tibio-femoral contact point moved 6 mm posteriorly on the tibial plateau during the descent phase of jumping reaching a most posterior position. During the ascent phase of jumping that followed, the contact point moved about 7 mm anteriorly from the most posterior position on the tibial plateau. During landing, from the most anterior position reached, the contact point traveled posteriorly on the tibial plateau about 10 mm, then anteriorly about 9 mm.

Comparisons between results of this work and other vertical jump and regular squat exercises results available in the literature were conducted.

2 Two-Dimensional Human Leg Anatomical Model

2.1 Kinematic Data. Musculoskeletal models are developed in order to capture and provide objective criteria for various movements [7]. The present model focuses on the vertical squat jump exercise. There are multiple factors that contribute to the execution of the movement such as muscular coordination, muscular strength, arm swing, and arm placement depending on the study [20].

The human leg model is composed of three bones, namely, femur, tibia, and patella. The knee is not modeled as a simple revolute joint. The entire motion is observed in a global coordinate system, which is a fixed XY coordinate system. Anatomical data to include articular geometry and insertion points of ligaments and muscles were given in their local coordinate systems, which are attached to the centers of mass of their respective bodies. OPENSIM was used to extract images, model *leg6dof9musc.osim*, in order to better grasp the geometry, anatomy, and the function of femur and tibia (Figs. 1 and 2). Muscle, ligament (Fig. 3), and contact forces' components are observed in their local coordinate systems, and later are transformed into components in the global coordinate system. Tibial orientation is given by θ_1 , the angle between the tibial longitudinal axis and positive horizontal X -axis, and femoral orientation by θ_2 , the angle between the femoral longitudinal axis and positive horizontal X -axis (Figs. 1 and 2). The overall motion is best described with respect to the tibiofemoral knee flexion angle $\theta_{TF} = \theta_2 - \theta_1$. Patellofemoral flexion angle θ_{PF} displays a linear behavior with respect to θ_{TF} [21–23]. Caruntu and Hefzy [21] developed a three-dimensional anatomically based dynamic modeling of the human knee to include both knee joints, tibio-femoral and patello-femoral. Their model was a forward dynamics model. They simulated the knee extension exercise and showed that for three different values of quadriceps force, the relationship between the patello-femoral flexion angle θ_{PF} and the tibio-femoral flexion angle θ_{TF} is as follows:

$$\theta_{PF} = \frac{7}{9} \theta_{TF} \quad (1)$$

In this work, we assumed the relationship between θ_{PF} and θ_{TF} given by Eq. (1) to hold. The direction of the patellofemoral contact force on the femoral condyle is given by θ_{PF} (Eq. (1)). The angle between the patellar tendon and the tibial shaft θ_{PT} , known

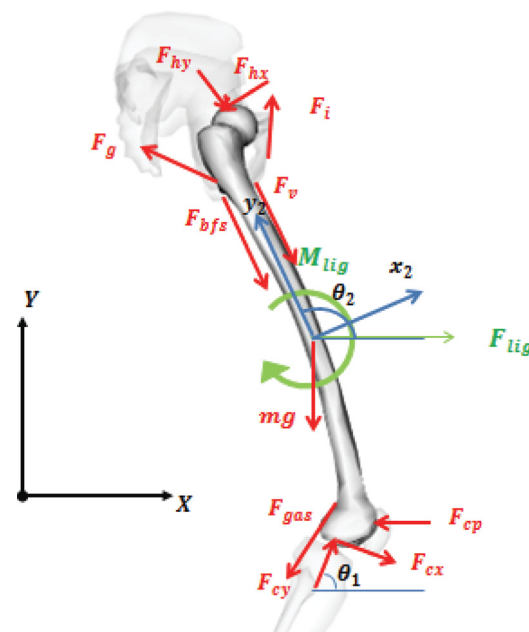


Fig. 1 Free body diagram of femur

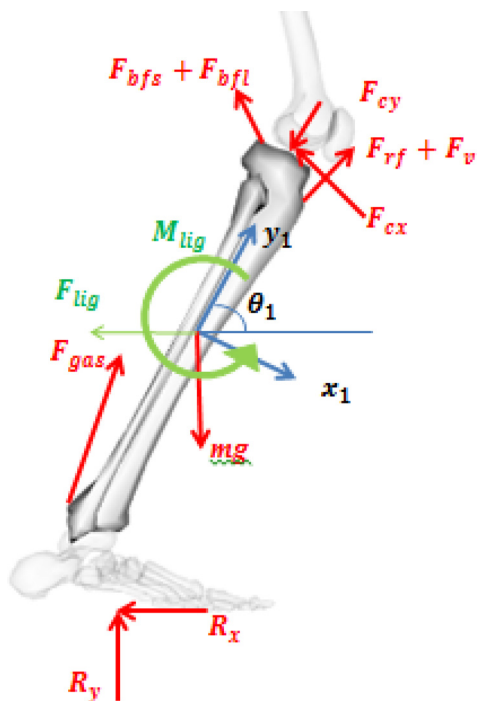


Fig. 2 Free body diagram of tibia

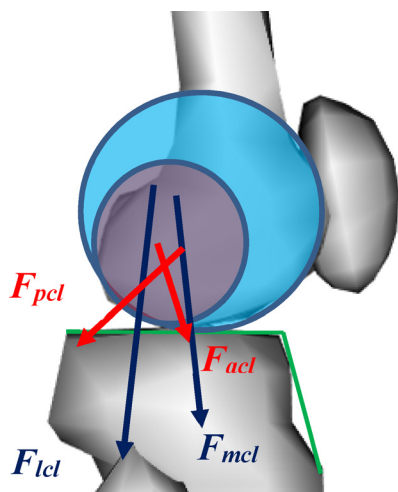


Fig. 3 Knee joint articular geometry model and ligament forces acting on femur

as PT sagittal plane angle, is a function of the flexion angle as given by DeFrate et al. [24] and Varadarajan et al. [25]

$$\theta_{PT} = \frac{\pi}{9} - \frac{3}{11}\theta_{TF} \quad (2)$$

Figure 4 displays the patello-femoral flexion angle θ_{PF} and the patellar tendon angle θ_{PT} as functions of the tibio-femoral flexion angle θ_{TF} (Eqs. (1) and (2)).

2.2 Knee Articular Surfaces. Knee femoral articular surface is modeled by two circles, one approximating the patello-femoral contact and the other one the tibio-femoral contact. The patello-femoral circle serves as reference for muscle insertions, patellar tendon orientation, and patello-femoral contact (Fig. 3). References [26–28] are used to estimate the patello-femoral circle, tibio-femoral circle, and the tibio-femoral contact point at 90 deg flexion

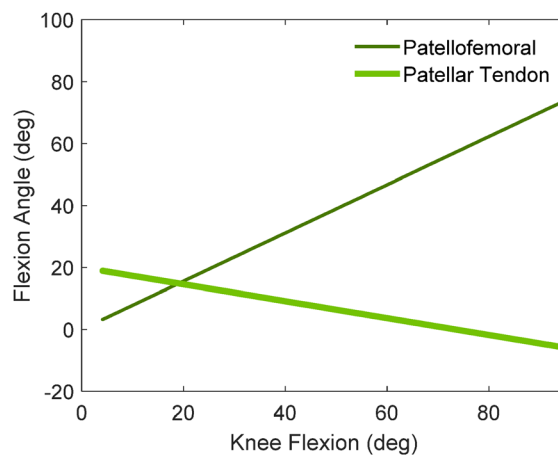


Fig. 4 Patello-femoral flexion angle and patellar tendon angle versus tibio-femoral knee flexion angle

angle, respectively. The radius of the patello-femoral circle is calculated using Yue et al. [26], which reports knee anthropometric data of Chinese, and white men and women. They reported the anteroposterior length of the femoral condyle between the two races. Assuming that the human bone structure is related to a person’s height, rather than race, a linear relationship is considered between anteroposterior length of the femoral condyle and the person’s height. The human subject of this work was 1.75 m tall and had a mass of 84 kg. It was calculated that the subject’s anteroposterior length of the femoral condyle is 7 cm, so the radius of the patello-femoral circle was 3.5 cm [26]. The tibio-femoral circle is used for the tibio-femoral center of rotation, contact point, and ligament insertions. The radius for the tibio-femoral circle was calculated using Granados [27] in which a 2D anatomical knee model was reported. The anatomical surfaces were based on the X-ray of a human subject. For this work, the X-ray was scaled up to match the antero-posterior length of the subject’s femoral condyle, then the curvature of the posterior side of the femoral condyle was traced using MATLAB and the radius of the tibiofemoral circle was found to be about 2 cm [27].

Finding the proper tibio-femoral center of rotation (COR) was an essential part, since this point is directly related to the ligament insertion points placement and the location of the tibio-femoral contact point. A virtual marker was added in order to adjust the COR to its proper location. The location of COR was determined using the tibio-femoral circle radius, acquired from Granados [27] and Hill et al. [28], where the posterior centers of the femoral condyles were measured during a squat exercise. COR was placed at a selected distance, anterior to the posterior edge of the tibial plateau. Specifically, it was placed on a direction perpendicular to the tibial plateau and above the tibio-femoral contact point (CTF) (Fig. 5). At 90 deg knee flexion angle, the location of CTF was $D = 2$ cm from the posterior edge of the tibial plateau [28]. COR was placed 2 cm distance from the tibial plateau on the perpendicular direction to the tibial plateau through CTF at 90 deg knee flexion.

The tibio-femoral COR location was then calculated with respect to the intercondylar marker (IM). The IM is a virtual marker located at the midpoint in the $x_2 y_2$ plane between the lateral and medial knee markers, which are denoted as LM and MM, respectively (Fig. 5). At 90 deg knee flexion, the polar coordinates with respect to IM of the tibiofemoral COR were calculated. The tibiofemoral COR coordinates were then calculated for all time frames of the exercise.

2.3 Leg Loads

2.3.1 Muscles. Muscles considered in this work, along with their insertions, are as follows: (1) gastrocnemius F_{gas} located between the femoral condyle and the calcaneus through the

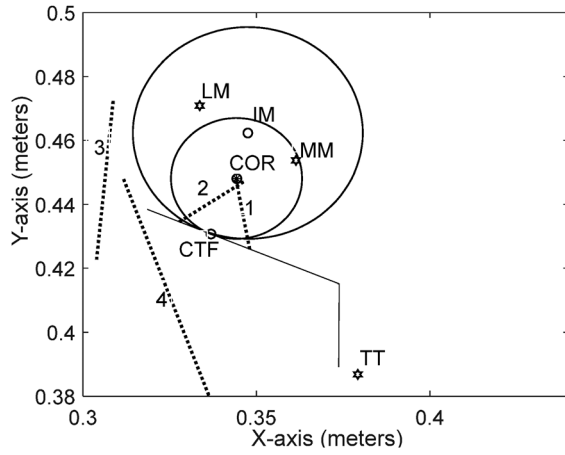


Fig. 5 Tibio-femoral COR calculation at 90 deg flexion, where TT is the tibial tuberosity marker and IM is the intercondylar virtual marker calculated as the midpoint between LM and MM, the lateral and medial condyle markers, respectively. Solid lines represent either the tibial plateau or the simplified knee condyle geometry, dashed lines represent the ligaments at that current position; 1, 2, 3, and 4 indicate ACL, PCL, LCL, and MCL, respectively.

Achilles tendon, (2) biceps femoris short head F_{bfs} between the fibula head and linea aspera and lateral supracondylar line of femur, (3) biceps femoris long head F_{bfl} between fibula head and ischial tuberosity, (4) rectus femoris F_{rf} between anterior inferior iliac spine and patella base, (5) gluteus F_g between iliac crest and posterior gluteal line and greater trochanter, (6) vasti F_v between femur and patella base, and (7) iliacus F_i between the region of the anterior inferior iliac spine and lesser trochanter. Hamstrings muscle force F_h and quadriceps muscle force F_q are given by

$$F_h = F_{bfl} + F_{bfs}, \quad F_q = F_{rf} + F_v \quad (3)$$

2.3.2 Knee Ligaments. There are four major knee ligamentous structures that hold the joint together. Ligaments are bone to bone connective tissues. They limit the relative displacement between femur and tibia. The four ligaments are ACL, PCL, LCL, and MCL, and their respective forces are denoted by F_{acl} , F_{pcl} , F_{lcl} , and F_{mcl} (Fig. 3).

The locations of the ligament insertion points were considered in the standing position [29]. The insertion points were then related to their respective body, i.e., femoral ligament points with respect to the tibiofemoral COR and the tibial ligament insertions with respect to the tibial plateau. The ligaments were modeled as nonlinear strings, providing force only in tension. The definition for the linear and nonlinear regions, slack lengths, and stiffness coefficients of the ligaments were acquired from Ref. [21]. The nonlinear behavior of ligaments is given by

$$(F^\ell)^n = \begin{cases} 0, & \varepsilon^n \leq 0 \\ (k^q)^n (L^n - L_0^n)^2, & \varepsilon^n < 2\varepsilon_0 \\ (k^\ell)^n [L^n - (1 + \varepsilon_0)L_0^n], & \varepsilon^n \geq 2\varepsilon_0 \end{cases} \quad (4)$$

where “ ε^n , $(k^q)^n$, $(k^\ell)^n$, L^n , L_0^n , and ε_0 are the strain, the stiffness coefficients for the quadratic and linear regions, the current length and slack length the n th ligament, and the threshold assumed to be 0.03, respectively” [21].

Only PCL force was not calculated using Eq. (4). Since the tibiofemoral center of rotation has an unusual behavior [30], the PCL was the only ligament largely affected. The marker-based approach captures the motion of the transepicondylar axis but not the geometric center axis, which depicts the true motion of the knee [30,31]. Due to this limitation, PCL was left to be found through

optimization along with muscle forces and contact forces, as shown afterward. However, PCL insertion points were anatomically based.

2.3.3 Contact Loads. Contact force is produced by contact of bones. There are three contact forces considered, namely tibio-femoral contact force, patello-femoral contact force, and hip joint contact force. The tibio-femoral contact force consists of two components: contact force parallel to the tibial plateau direction F_{cx} and perpendicular to the tibial plateau F_{cy} . The hip contact force components are perpendicular to the femoral longitudinal direction F_{hx} and parallel to the femoral longitudinal direction F_{hy} . All muscles and ligaments provide forces only being in tension and bone contact only in compression.

There are some assumptions to simplify this model. First, the patellar tendon orientation is given by DeFrate et al. [24] and its force is equal to the quadriceps force which is given by Eq. (3). Second, although patella is not included as a third body in the investigation, the patello-femoral contact force F_{cp} is included in the model. Third, F_{gas} and F_{cy} are parallel to the longitudinal axis of tibia [32,33], and F_{cx} is zero due to negligible friction on the tibial plateau [34]. Fourth, the force F_h is parallel to the femoral longitudinal axis [35]. Fifth, the geometrical center of the femoral condyle has a trajectory parallel to the tibial plateau [31].

2.4 Equations of Motion. Figures 1 and 2 depict the free body diagrams of tibia and femur for a current moment in time during the exercise. The equations of motion are written in the sagittal plane using Newton’s second law on the X and Y directions, and Euler equation on the Z direction for each body. The equations of 2D motions of tibia and femur are

$$\sum F_{Xi} = m_i \times a_{XCi}, \quad \sum F_{Yi} = m_i \times a_{YCi}, \quad \sum M_{Ci} = I_{Ci} \times \alpha_i \quad (5)$$

where subscripts are $i = 1$ for tibia, $i = 2$ for femur, C for center of mass; F_{Xi} , F_{Yi} , M_{Ci} , and I_{Ci} are forces, moments, and moments of inertia, respectively; and a_{XCi} , a_{YCi} , and α_i are linear accelerations of C and angular accelerations of the corresponding bodies, respectively. Equations (5) can be rewritten as

$$\begin{aligned} R_{Xi} &= \left(\sum F_{Xi} \right)_{\text{int}} = m_i \times a_{XCi} - \left(\sum F_{Xi} \right)_{\text{ext}}, \\ R_{Yi} &= \left(\sum F_{Yi} \right)_{\text{int}} = m_i \times a_{YCi} - \left(\sum F_{Yi} \right)_{\text{ext}}, \\ T_i &= \left(\sum M_{Ci} \right)_{\text{int}} = I_{Ci} \times \alpha_i - \left(\sum M_{Ci} \right)_{\text{ext}} \end{aligned} \quad (6)$$

where R_{Xi} , R_{Yi} , and T_i are the resultant intersegmental (knee and hip) forces and moments; $\left(\sum F_{Xi} \right)_{\text{ext}}$, $\left(\sum F_{Yi} \right)_{\text{ext}}$, and $\left(\sum M_{Ci} \right)_{\text{ext}}$ are the external forces on tibia (and foot) and femur; and $\left(\sum F_{Xi} \right)_{\text{int}}$, $\left(\sum F_{Yi} \right)_{\text{int}}$, and $\left(\sum M_{Ci} \right)_{\text{int}}$ are the internal forces given by ligament, contact, and muscle forces on the respective body [36].

2.5 Inverse Dynamics. An inverse dynamics human leg model is developed and used in this work. Finding the muscle forces and internal loads during the exercise is the overall goal [19]. The motion of the subject during the exercise was captured using a Vicon motion analysis system. These data were acquired in the Biomechanics Laboratory at the University of Texas Rio Grande Valley. The experimental data were used to calculate the input data for the inverse dynamics model. The input data consisted of (1) coordinates of the femoral and tibial centers of mass, (2) the orientations of tibia and femur, (3) their corresponding accelerations, and (4) ground reaction forces. The first step was to calculate the intersegmental forces and moments R_{Xi} , R_{Yi} , and T_i , Eq. (6), for each joint and time frame using the experimental data. Forces were calculated by considering each segment, iteratively, moving from tibia plus foot, proximally along the kinetic chain

[37]. The system of equations of the model has a large number of unknowns to include muscle forces and contact forces [38–40]. Specifically, the unknowns are nine muscle forces to include F_{bfl} , F_{bfs} , F_{rf} , F_v , F_g , F_i , and F_{gas} , and F_h and F_q , see Eq. (3), four contact forces F_{hx} , F_{hy} , F_{cy} , and F_{cp} , one ligament force F_{pcl} , and the location of the tibio-femoral contact point on the tibial plateau given by distance D . These forces are internal forces and they have as resultants $(\sum F_{Xi})_{int}$, $(\sum F_{Yi})_{int}$, and $(\sum M_{Ci})_{int}$ which are the intersegmental forces and moments in Eqs. (6). Intersegmental forces and moments are already calculated from the experimental data. This is an underdetermined system since the number of equations is lower than the number of unknowns. Such system has an infinite number of possible solutions. To find a solution of the inverse dynamics model, the optimization method used an objective function that was minimized under given constraints. Several objective functions can be formulated for minimization of the forces in the muscles, the work done by the muscles, reactions at the joints, moments carried by the ligaments at the joints [38], muscle forces and moments at all joints [41], muscle stresses [42–44], and metabolic energy expended per unit distance traveled [45].

The objective function [38–40,46] to be minimized in this work includes muscle forces, contact forces, and the PCL force

$$\begin{aligned} \min f = & F_{bfl}^2 + F_{bfs}^2 + F_{rf}^2 + F_v^2 + F_g^2 + F_i^2 + F_{gas}^2 + F_{pcl}^2 + F_{cp}^2 \\ & + F_{cy}^2 + F_{hx}^2 + F_{hy}^2 \end{aligned} \quad (7)$$

with the unknowns satisfying the following inequality constraints:

$$\begin{aligned} F_{bfl} \geq 0, F_{rf} \geq 0, F_{cx} = 0, F_{cy} \geq 0, F_g \geq 0, F_i \geq 0, F_{hx} \geq 0, \\ F_{hy} \geq 0, F_v \geq 0, F_{bfs} \geq 0, F_{gas} \geq 0, F_{cp} \geq 0, F_{pcl} \geq 0, D \geq 0 \end{aligned} \quad (8)$$

and equality constraints given by Eqs. (6). D is the distance between the tibio-femoral contact point and the posterior edge of the tibial plateau.

3 Experimental Protocol

3.1 Biomechanics Motion Instrumentation. The experimental data were gathered using two AMTI force plates, Advanced Mechanical Technology Inc., Watertown, MA, and ten Vicon MX T-Series infrared cameras, Vicon, Centennial, CO. The AMTI force plates, each measuring 60 cm × 60 cm, provided the ground reaction forces in the X , Y , and Z directions, moments about the X , Y , and Z directions, and centers of pressure in the XZ -plane. The sampling rate for the AMTI force plates was 1000 Hz.

The ten infrared cameras captured the light reflected by the markers as the subject performed the task. The Vicon system recorded all marker locations at a rate of 100 Hz and provided the coordinates of each marker coordinates to be used in the present model. Both sets of equipment are shown in Fig. 6.

3.2 Protocol. The human subject was required to perform a warm-up exercise and dynamic stretching before conducting the test. The warm-up exercise consisted of walking lunges, high knees, and practice vertical jumps. Once completing the 5 min warm-up routine, the subject was instructed to complete the vertical jump test protocol. The procedure was composed of five maximal vertical jumps. This is a test based on contact and air time [6].

The vertical jump in this work is a CMJ with no arm swing. The CMJ started from the upright standing position and transitioned through instructed phases to replicate the exercise. Two positions are illustrated in Fig. 7. The arms are kept akimbo (arms placed on the hips and elbows faced outward) in order to mitigate any momentum in the CMJ similar to Ref. [5]. However, in Fig. 7, the arms are not showed akimbo for the only reason of having a good lateral view of the markers. Additionally, the initial descent

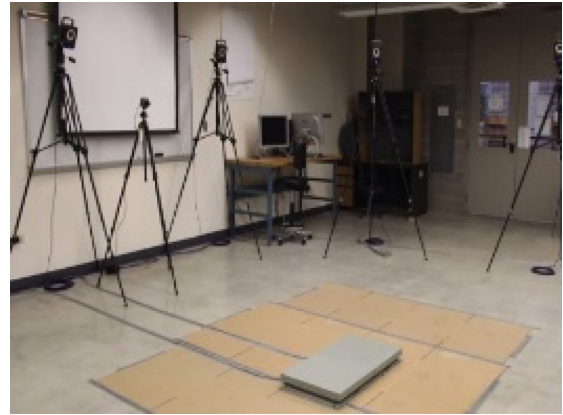


Fig. 6 Biomechanics laboratory (Director Caruntu) at University of Texas Rio Grande Valley

phase was performed at a slower pace to further limit any loading. The depth of the squat of jumping was measured between the ground and the hip and measured when the subject's knee flexion angle was approximately 95 deg [6]. The subject was instructed to hit the same descent marker before every vertical jump. The subject was asked for a fast ascent phase, jump for a maximum height, and soft landing. A soft landing was accomplished by performing another squat once the feet touch down in a toe-heel landing progression. If not all the requirements were met, the trial was discarded and repeated after the appropriate rest interval. After every test, completed or failed, the subject waited 2 min before attempting another trial. This was done to avoid any fatigue that might be encountered.

3.3 Markers. The marker set employed in this study comprises markers on pelvis, thigh, calf, and foot [5,37]. Reflective markers were placed on bone landmarks of the subject (Figs. 7 and 8). Their placements were most distal point on the toe, heel, lateral and medial ankle, lateral and medial knee condyles, tibial tuberosity, hip, and the front and rear of the pelvis. Shells of four markers were placed on the foot, shank, and thigh. These shells were used when the capture experienced a “gap” in the data. The shells aided the software to calculate the missing position of the marker. Gaps are instances where the marker was not captured, which may be due to marker being covered. The captured data were used for the input data to the knee model.

The segment lengths, centers of mass, radii of gyration, and moments of inertia of tibia and femur were calculated using subject's mass and height and anthropometric data [47–49].

3.4 Data Filtering. The experimental data were captured and processed using the VICON NEXUS software. Collected data were then exported onto an excel spreadsheet where the marker data

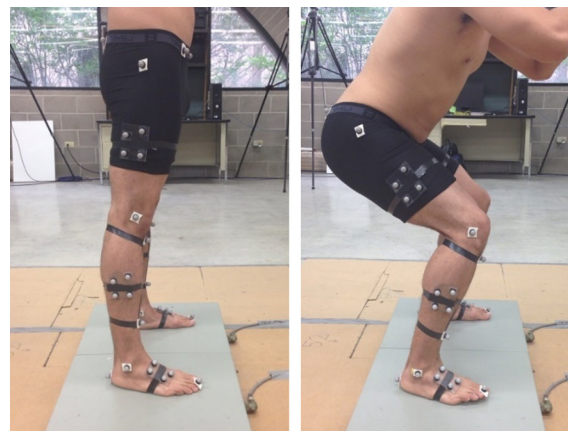


Fig. 7 Positions during the vertical jumps

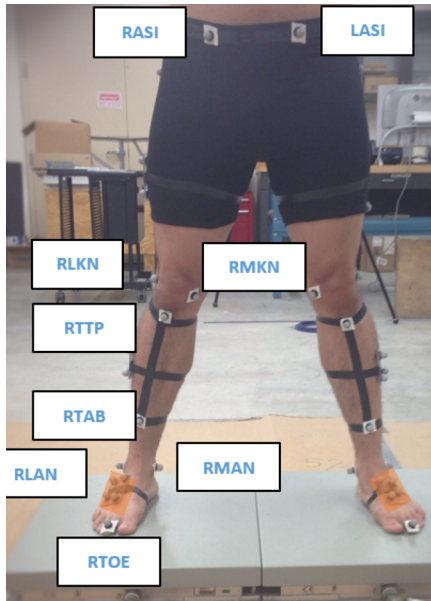


Fig. 8 Marker placement

and the force plate data were compiled. These data were used as input data for the 2D human leg anatomical inverse dynamics model. The collected data (raw data) were filtered using a low-pass, fourth-order, zero-lag Butterworth filter [47,50] with a cutoff frequency of 30 Hz [51,52], resulting from residual analysis [47] of the experimental data.

Linear velocities $v_{i+1/2}$ and accelerations $a_{i+1/2}$ of the centers of mass, and angular velocities $\omega_{i+1/2}$ and accelerations $\alpha_{i+1/2}$ were calculated halfway between sample times [47]. The frame rate is 100 Hz; therefore, Δt is 0.01 s. These accelerations were then used as input data for the equation of motion for the 2D model. The equations of motion were equality constraints in the inverse dynamics model used in this work.

4 Numerical Simulations

Numerical simulations were conducted using the inverse dynamics model. (1) The vertical jump exercise is compared to the other studies with similar procedure and (2) its descent phase of jumping is also compared with the descent phase of regular squat exercise. The reason for this last comparison is that the descent phase of jumping is similar to some extent to the regular squat. For the vertical jump exercise, only jumping and landing are of interest. The standing position and airborne times are not included.

Figures 9 and 10 show the vertical coordinate of the hip joint (greater trochanter marker), and the ground reaction forces during the exercise, respectively. In Fig. 9, the vertical coordinate of the hip joint decreases from about 0.89 m to 0.60 m between $t = 1.40$ s and $t = 2.22$ s and then the vertical coordinate of the hip increases from 0.60 m to 1.20 m between 2.22 s and 2.90 s. Therefore, the subject jumps 0.3 m above the standing position. During landing, at $t = 3.26$ s, the vertical coordinate of the hip reaches a lowest value of 0.80 m, and at $t = 3.50$ s, the hip reaches 0.88 m.

Figure 10 shows the vertical GRF, vertical R_y , and anterior-posterior R_x on one leg. Vertical force R_y is significant in this exercise and has bimodal peaks, indicating the toe heel landing style [9]. The largest GRFs are right before the take-off and right after landing. At $t = 1.00$ s, R_y has a value of 0.50 BW, which corresponds to standing and keeps this value until $t = 1.27$ s, and then R_y decreases to a minimum of 0.34 BW at $t = 1.40$ s. Next, R_y continuously increases to reach a maximum of 1.10 BW at $t = 2.60$ s and then quickly decreases to zero at $t = 2.66$ s. The interval of time when the subject is airborne is

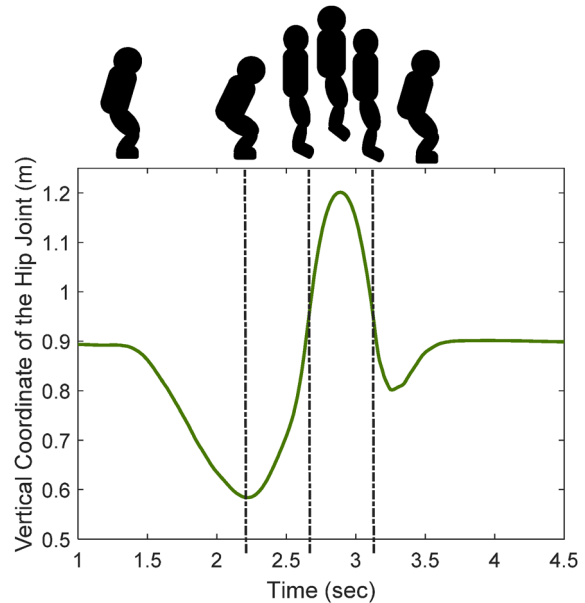


Fig. 9 Vertical coordinate of the hip joint

between $t = 2.66$ s and $t = 3.10$ s. At $t = 3.15$ s, R_y reaches a maximum of 2.70 BW, then decreases to 1.10 BW and again increases, now to a local maximum of 1.60 BW at $t = 3.20$ s. The force R_y then decreases to reach a minimum of 0.35 BW at $t = 3.50$ s. Then, it continues to slowly increase to 0.54 BW and then decrease to 0.50 BW at $t = 3.80$ s and $t = 4.40$ s, respectively.

Figure 11 shows the knee flexion angle and the important stages of the exercise marked by vertical lines. The flexion angle reaches a maximum of 95.4 deg during jumping and 55.4 deg during landing. The progression of the exercise is marked by small subject figures on top of the graphs and vertical lines for important transition times. The first vertical line at $t = 2.22$ s marks the lowest point (the largest knee flexion angle) of the descent phase of jumping. This is the time of the transition from the descent to the ascent phase of jumping. The second vertical line at $t = 2.66$ s shows the instant when the subject takes off and goes airborne.

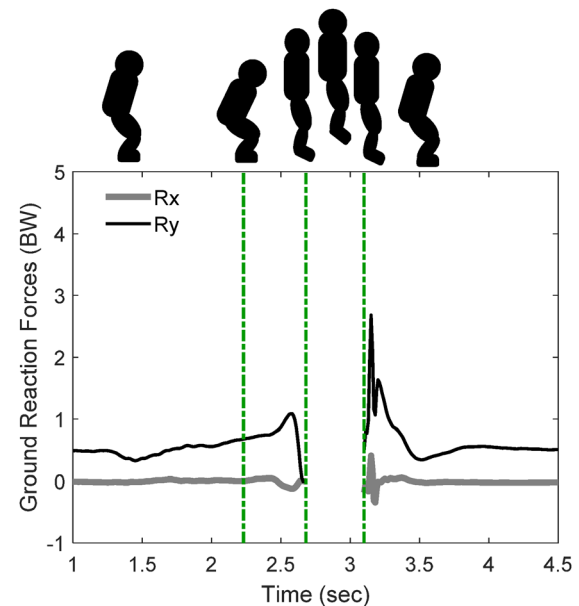


Fig. 10 Experimental ground reaction forces during the vertical jump exercise

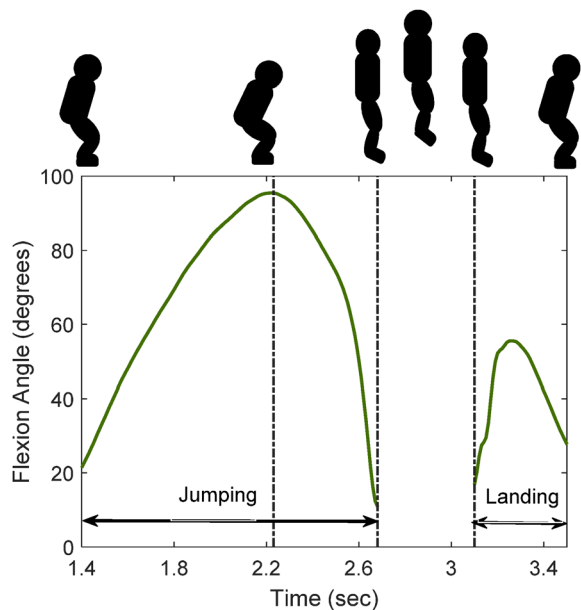


Fig. 11 Experimental knee flexion angle during the vertical jump exercise

The third vertical line at $t = 3.10$ s marks the instant when the subject lands. The progression of the exercise is also marked in Figs. 11–17.

The cycle of the vertical jump exercise is defined as follows. The beginning of the exercise is considered when the vertical ground reaction force reaches its minimum in the descent phase of jumping, specifically when the time $t = 1.40$ s (Fig. 10). One can see from Fig. 9 that this is the time when the descent phase starts. The end time of this exercise is considered when the vertical ground reaction force reaches its minimum in the landing phase of the exercise, specifically when the time $t = 3.50$ s, in Fig. 10. One can see that at this time, the subject almost reaches the standing position. From Figs. 9 and 11, one can notice that the time for the lowest squatting position (largest flexion angle) of jumping occurs

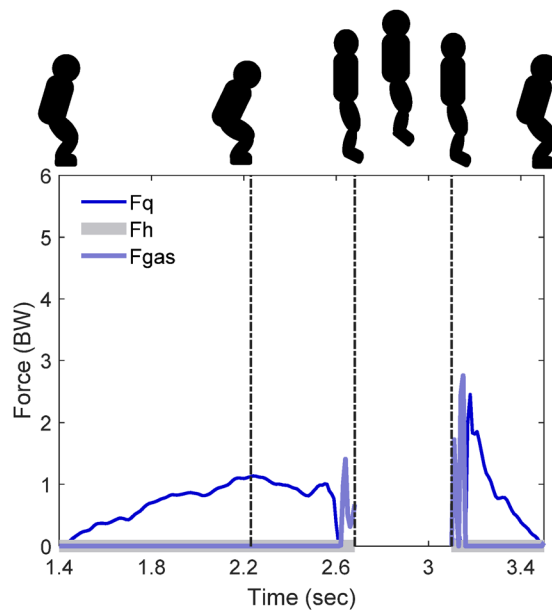


Fig. 13 Quadriceps, hamstrings, and gastrocnemius muscle forces during the vertical jump exercise

at $t = 2.22$ s and the time for the lowest squatting position of landing occurs at $t = 3.27$ s.

Figure 12 illustrates the angles θ_2 and θ_1 between femoral and tibial longitudinal axes and the positive global horizontal x -axis. The knee flexion angle in Fig. 11 was calculated as $\theta_{TF} = \theta_2 - \theta_1$.

Figure 13 shows the quadriceps, hamstrings, and gastrocnemius muscle force production, where the quadriceps and hamstrings are the combination of components as described in Eq. (3). The quadriceps muscle is the main contributor to the vertical jumping being active throughout the entire exercise. During jumping, it increases from zero reaching 1.10 BW at the lowest descent position of jumping (largest knee flexion angle), decreases to 0.80 BW, and then increases to a maximum of 1.00 BW before the take-off.

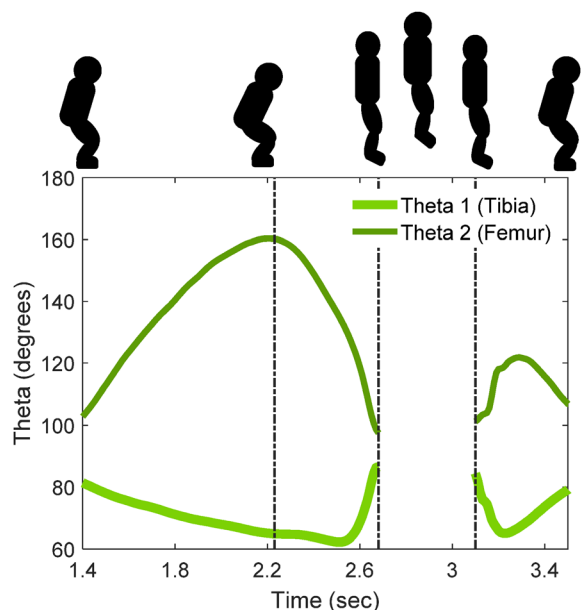


Fig. 12 Experimental tibial and femoral angles θ_1 and θ_2 , respectively, with respect to the horizontal axis during the vertical jump exercise

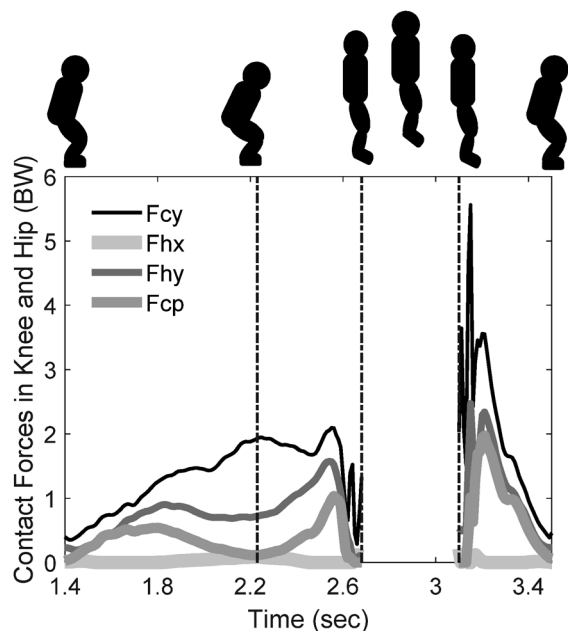


Fig. 14 Contact forces during the vertical jump exercise, tibio-femoral contact force F_{cy} , hip contact forces F_{hx} and F_{hy} , and patello-femoral force F_{cp}

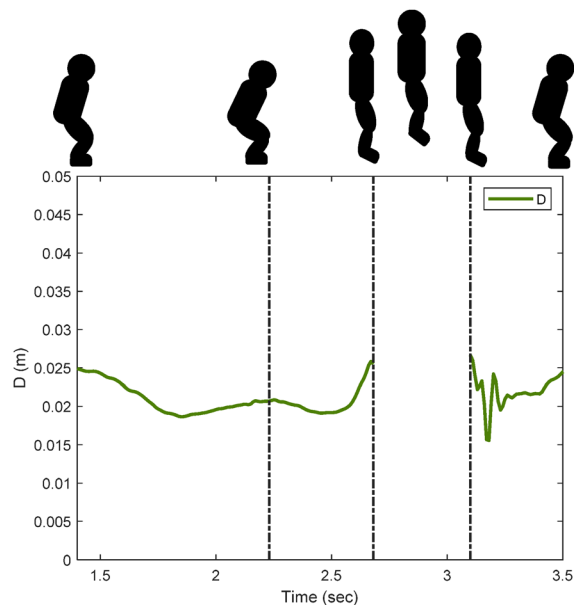


Fig. 15 Motion of tibio-femoral contact point during the vertical jump exercise

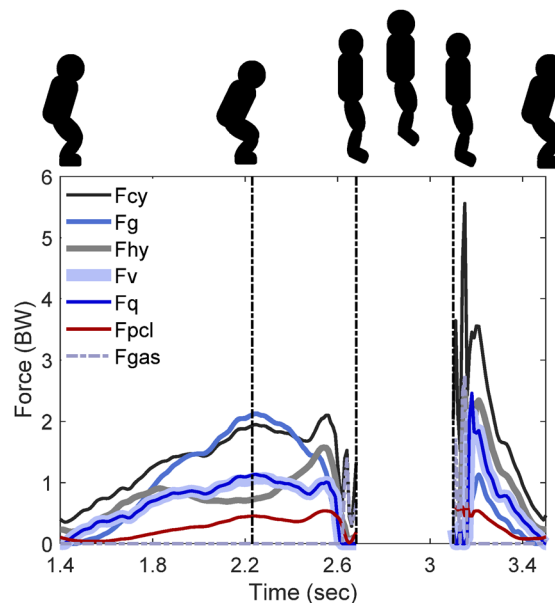


Fig. 17 All significant forces during the vertical jump exercise

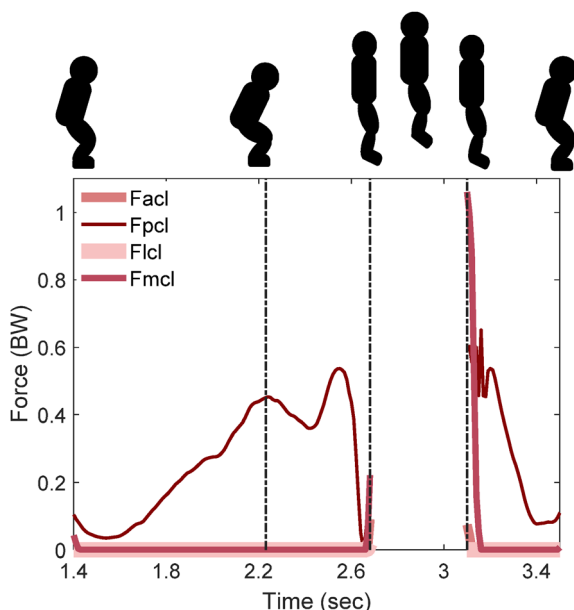


Fig. 16 Ligament forces during the vertical jump exercise

During landing, in the first part of landing, the quadriceps muscle experiences a force of about 2.50 BW. The gastrocnemius muscle force is not significant during the exercise, except right before the take-off when it reaches around 1.40 BW and in the first part of landing when it reaches 2.80 BW.

Figure 14 depicts the contact forces experienced in the hip and the knee. The tibio-femoral normal contact force F_{cy} is the highest of the five contact force components predicted by the present model. During jumping, (1) F_{cy} reaches two maxima, 2.00 BW at the lowest descent position of jumping and 2.10 BW right before the take-off; (2) the hip contact force F_{hy} reaches a local maximum of 0.9 BW during the descent phase, a local minimum of 0.71 BW at the lowest descent position of jumping, and a maximum of 1.60 BW right before the take-off; (3) the patello-femoral contact force F_{cp} has the same pattern as the contact force in the hip, reaching a local maximum of 0.54 BW during the descent

phase of jumping and a maximum of 1.00 BW right before the take-off. During landing, in the first part of it, (1) F_{cy} experiences a maximum of 5.60 BW, (2) F_{hy} which is parallel to the femoral longitudinal axis reaches a maximum of 2.50 BW and shortly another local maximum of 2.30 BW. F_{hy} experiences a force of 0.23 BW at the end of the exercise, $t = 3.50$ s. (3) In the first part of landing, F_{cp} reaches a maximum of 2.00 BW. Then, it decreases to zero by the end of the exercise, $t = 3.50$ s. The force F_{cp} is in agreement with Cleather et al. [5] who reported the same pattern and maxima of 3.20 BW and 3.30 BW during jumping and landing, respectively. Their larger maximum values are due to (1) the subject, male athletes [5] versus a recreational athlete in this work, (2) jump height, 0.40 m [5] versus 0.30 m in this work, and (3) different time intervals, jumping time 0.75 s [5] versus 1.26 s in this work, and landing time of about 0.30 s [5] versus 0.40 s in this work.

Figure 15 illustrates the motion of the tibio-femoral contact point during the exercise, where D is the tibial distance between the tibio-femoral contact point and the posterior edge of the tibial plateau. During jumping, the contact point moves 6 mm posteriorly on the tibial plateau during the first half of the descent phase of jumping, then 2 mm anteriorly as the subject reaches the lowest position of jumping, 2 mm posteriorly during the first half of the ascent phase, and another 7 mm anteriorly during the second half of the ascent phase. During landing, the contact point travels posteriorly 10 mm from the most anterior position (same location as right before the take-off), then 8 mm anteriorly followed by 4 mm posteriorly, and then another 5 mm anteriorly settling to the same position as when the entire exercise started. The take-off of jumping and the beginning of landing find the tibiofemoral contact point with respect to the tibial plateau in the most anterior position. The same pattern of the contact point is observed for both jumping and landing. However, landing experiences a faster change in the location of the contact point. This is due to much shorter landing time than the jumping time. The distance traveled by the contact point on the tibial plateau is less than or equal to 10 mm.

Figure 16 illustrates the ligament forces in the knee. The ligament with the most activity is the PCL. During jumping, the maximum PCL forces are 0.45 BW and 0.54 BW at the lowest position (maximum flexion angle of jumping) and right before take-off, respectively, and the MCL which is active for a very short period of time right before the take-off reaching a maximum of 0.22 BW. During landing, in the first phase of it, the maximum PCL force is

0.65 BW and the maximum MCL force is 1.10 BW. Forces in PCL are relatively low when compared to contact forces and some of the muscle forces. The maximum force in the PCL is much less than the failure limit for healthy subject PCL which is around 4.5 kN [5], i.e., about 5.50 BW. PCL is in tension when posterior shear occurs [5]. The pattern of PCL force during the exercise is in good agreement with posterior shear force reported in the literature [5]. Again, differences between magnitudes in this work and Ref. [5] are due to (1) the type of athlete, (2) jump height, and (3) different jumping and landing time intervals, see the discussion of Fig. 14. The other two ligaments, ACL and LCL, do not show any significant activity during the vertical squat jump.

Significant forces of the vertical squat jump are shown in Fig. 17, tibio-femoral normal contact force F_{cy} in the knee, hip contact force F_{hy} , gluteus muscle force F_g , quadriceps muscle force F_q , gastrocnemius muscle force F_{gas} , and PCL force. Gluteus muscle force is a very important force throughout the exercise. Gluteus muscle has the largest force in the system, 2.12 BW for the lowest position of jumping, and a significant value of 1.13 BW during landing.

From the present data, the greatest magnitudes of the significant forces in this exercise are experienced during jumping, right before the take-off, and right after landing. However, gluteus muscle reaches its maximum at the largest knee flexion angle during jumping. The knee was the joint that experienced most of the loads, contact and supporting muscles.

5 Discussion and Conclusion

In this work, a sagittal plane, inverse dynamics, model of human leg was developed in order to investigate contact, muscle, and ligament forces, and tibio-femoral contact point motion during vertical jump exercise. Experimental data, collected in the biomechanics laboratory at the University of Texas Rio Grande Valley, were used as input data for the inverse dynamics model. The vertical jump exercise consists of three phases, namely jumping, airborne subject, and landing. The novelty of this work is related to vertical jump exercise with a larger completion time of the jumping phase and consists of (1) predicting the tibio-femoral, patello-femoral, and hip joint contact forces, and quadriceps and hamstrings muscle forces. This investigation also reports, for the entire duration of the vertical jump exercise, (2) the motion of the tibio-femoral contact point on tibial plateau, (3) gastrocnemius and (4) gluteus muscle forces, and (5) cruciate and collateral ligaments' forces.

All contact forces, and quadriceps muscle force, experience peak values during the ascent phase of jumping and the first part of landing. The largest peak values during these two phases belong to tibio-femoral contact force, jumping 2.10 BW and landing 5.60 BW. The contact forces for jumping, predicted in this work, have the same pattern, but lower values than data reported in the literature. This is due to larger jumping time in this work. However, the contact forces for landing are in very good agreement with data reported in the literature, since the landing time was similar.

During the vertical jump, the tibio-femoral contact point, Fig. 15, travels posteriorly on the tibial plateau for the descent phases of jumping and landing, 6 mm and 9 mm, respectively. During both ascent phases, before the take-off and the terminal phase of landing, the contact point travels anteriorly, 7 mm and 9 mm, respectively; at the end of the exercise, the contact point is back to its original position during standing.

The level of activation of the hamstrings muscle during the exercise is not significant (Fig. 13). This does not contradict data reported in the literature for muscle activation patterns during squat exercise [53]. Their experimental electromyography data in terms of normalized muscular activity show that during squat exercise the hamstrings has only a level of activation of 6–7% of its maximum voluntary isometric contraction during the descent phase and only 7–11% during the ascent phase, while the

quadriceps reaches 100% of its maximum voluntary isometric contraction. Spagele et al. [7] reported as well a very small level of hamstrings normalized muscle excitation during the exercise.

Gluteus and gastrocnemius muscle forces show different levels of activation (Fig. 17). The gluteus muscle force F_g is activated during the entire vertical jump exercise, reaching a peak of 2.10 BW in the lowest position of the descent phase of jumping and about 1.12 BW during landing. The gastrocnemius muscle force is not activated during the entire exercise, except right before the take-off when it reaches a peak of 1.40 BW, and during the first phase of landing, when it reaches a peak of 2.80 BW.

Posterior cruciate ligament and MCL show significant level of activation during vertical jump exercise. PCL is activated during the entire exercise showing two peaks during jumping, one peak of 0.45 BW at the lowest jumping position and 0.55 BW right before the take-off, and one peak of 0.65 BW during the first phase of landing. MCL shows rather no significant activity during jumping, but shows a peak of about 0.90 BW during the first phase of landing. ACL and LCL show no significant level of activation during the exercise.

5.1 Comparisons of Vertical Jump Predictions With Data Reported in the Literature

In this section, a comparison between this work and data reported in the literature [5,19] is conducted. There are some differences between type of subjects and type of performance during the exercise. Athletic males jumped as high as 0.40 m in Ref. [5], and basketball players jumped as high as 0.50 m in Ref. [19], while in this work the exercise was performed by a recreational athlete who jumped only 0.30 m. Figure 18 gives details regarding the completion times as well.

In Figs. 18–21 the zero time for all data is the time when the ground reaction forces reached a minimum during jumping, since the exercise cycle was defined as the time between the minimum vertical ground reaction force during the descent phase of jumping and the minimum vertical ground reaction force during landing. Therefore, one is able to compare the same exercise but with different completion times.

Figure 18 displays a comparison with data available in the literature [5,19] of the vertical component of the ground reaction forces R_y produced during the vertical squat jump exercise. In the vertical axis, the ground reaction force units are converted into terms of BW. This allows for a proper comparison. The horizontal axis shows time in seconds. In Refs. [5], [19] and present work, total completion times are 1.75 s, 1.80 s, and 2.10 s, jumping times 0.75 s, 0.93 s, and 1.26 s, landing times 0.50 s, 0.50 s, and 0.40 s, and airborne times 0.45 s, 0.40 s, and 0.30 s, respectively. Present work has the largest total and jumping completion times, similar landing time, and lowest airborne time. Figure 18 shows a good

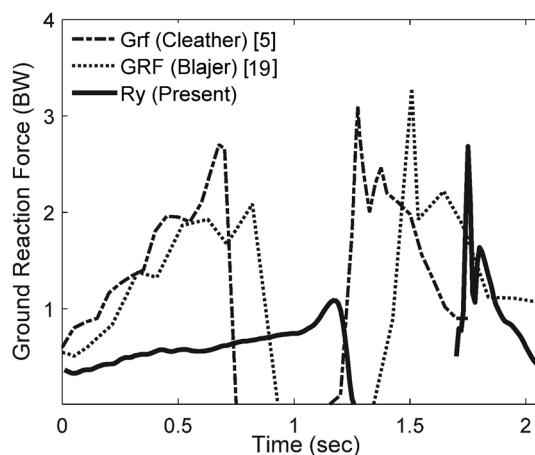


Fig. 18 Vertical ground reaction force R_y , comparison for the vertical jump exercise

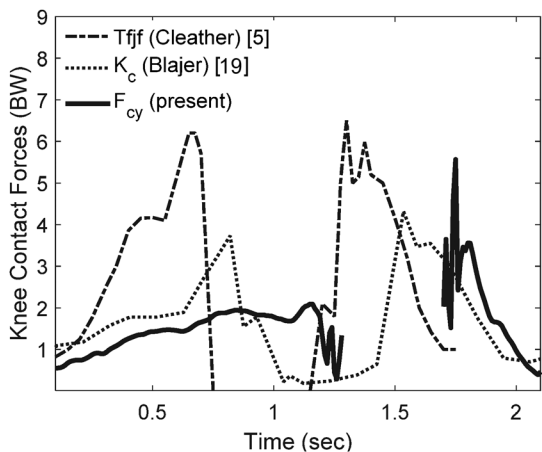


Fig. 19 Tibio-femoral contact force, comparison for the vertical jump exercise

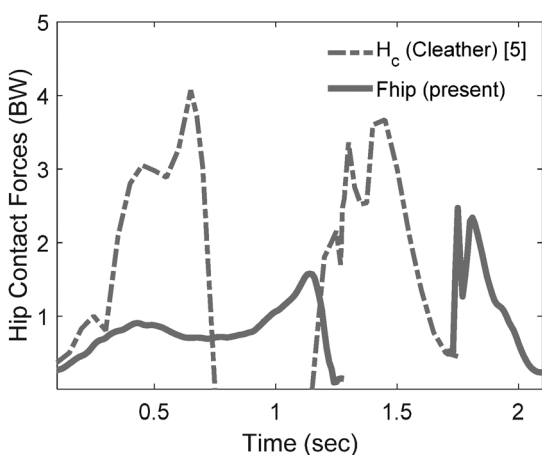


Fig. 20 Hip contact force, comparison for the vertical jump exercise

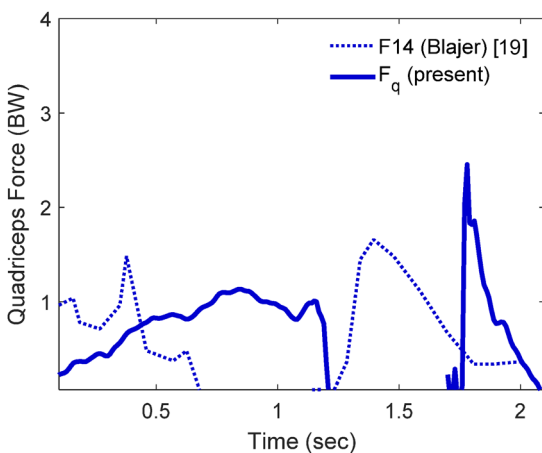


Fig. 21 Quadriceps force, comparison for the vertical jump exercise

agreement of this work with data reported in the literature. The patterns are similar, the largest force magnitudes occurred right before the take-off and right after landing. In Refs. [5], [19] and present work, the maximum values of jumping ground reaction forces are 2.70 BW, 2.10 BW, and 1.10 BW, and the maximum

values of landing ground reaction forces are 3.10 BW, 3.30 BW, and 2.70 BW, respectively. While the maximum values of landing ground reaction forces are similar to some extent due to similar landing times, the maximum values for jumping ground reaction forces are quite different due to large variations between the jumping times of the three investigations. For shorter jumping completion time, the contact forces have higher values as in Ref. [5], while for longer jumping completion time, the contact forces have lower values as in this work. The maximum height the subject reached during the exercise influenced the ground reaction forces as well.

Figure 19 depicts a comparison of the predicted tibio-femoral normal contact force F_{cy} with data available in the literature. The tibio-femoral contact force parallel to the tibial plateau F_{cx} is zero, due to very low friction coefficient. The predictions of present investigation regarding tibio-femoral normal contact force F_{cy} are in agreement with data reported in the literature [5,19]. All show similar patterns during the exercise. The maximum contact force F_{cy} occurs right before the take-off and right after landing. In Refs. [5,19] and this work, the maximum values of tibio-femoral contact force during jumping are 6.20 BW, 3.70 BW, and 2.10 BW, and the maximum values of tibio-femoral contact force during landing are 6.50 BW, 4.30 BW, and 5.60 BW, respectively. The maximum values of F_{cy} during jumping are different due to (1) type of athlete, (2) completion times, and (3) largest height attained during the exercise, while the maximum values of F_{cy} during landing are similar due to similar landing times.

Figure 20 illustrates a comparison of the resultant hip contact force F_{hip} to data reported in the literature. The components of the hip contact forces were combined $F_{hip} = \sqrt{F_{hx}^2 + F_{hy}^2}$. However, the contact force perpendicular to the longitudinal axis of the femur F_{hx} was so minute that it made little difference. The hip contact forces predicted by the present investigation are in agreement with Ref. [5]. They show the same pattern. The maxima occur right before the take-off and right after landing. The maximum values during jumping are 4.10 BW [5] and 1.60 BW in present work, and during landing are 3.70 BW and 2.50 BW in present work. Again, the differences in maximum values are due to (1) type of athlete, (2) completion times, and (3) largest height attained during the exercise.

Figure 21 illustrates a comparison between the quadriceps force F_q of this study and data available in the literature [19]. The resulting data of the two investigations show a similar progression throughout the exercise. Both investigations, Ref. [19] and this work, reported similar peaks during jumping 1.50 BW and 1.10 BW, and right after landing 1.70 BW and 2.50 BW, respectively. This work is in agreement with data reported in the literature. Differences are due to the type of athlete and the way the exercise was performed.

5.2 Tibio-Femoral Contact Point—Comparison of Descent Phases of Vertical Squat Jump and Regular Squat Exercises. Since the vertical jump exercise is derived from a squat progression, the descent phases of regular squat and vertical jump can be compared. The ascent phase is not subject of comparison since the vertical jump exercise is performed at a faster rate and higher intensity than the regular squat exercise. Figure 22 depicts the location of the contact point on tibia during the vertical jump in this work and that of regular squat exercise [54]. References [26] and [27] were used to determine the femoral geometry, and Ref. [28] to determine the location of the tibiofemoral contact point at 90 deg knee flexion. Then, calculations of the locations of the tibiofemoral contact point were carried over to the rest of the positions. The progression of the contact point is in good agreement with Ref. [54] for the first half of the descent phase of jumping. For the second half of the descent phase, there is a difference. One should mention that Mukarami et al. [54] used healthy males performing squats under periodic X-ray images at a rate of 10 frames per second. They analyzed the in vivo three-dimensional

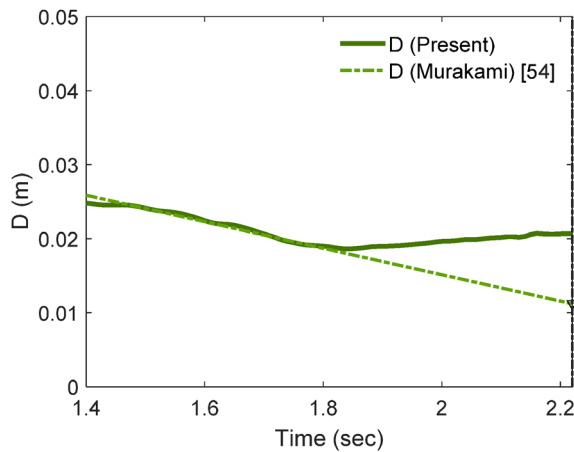


Fig. 22 Motion of tibio-femoral contact point, comparison for squat data during descent phase of vertical jump exercise. D is the tibial distance between the contact point and the tibial posterior edge.

kinematic parameters of subjects' knees, namely the tibio-femoral flexion angle, antero-posterior translation, and internal-external rotation, using serial X-ray images. The model in this work is a 2D model, so it does not account for the internal-external rotation of the knee, namely the screw home mechanism, which is significant in the second half of the descent phase of jumping.

5.3 Conclusion. The present investigation offers new insight regarding internal forces during the vertical jump exercise, a countermovement jump [55]. Present work used experimental ground reaction forces as well as motion analysis data, and predicted the tibio-femoral, patello-femoral, and hip joint contact forces, as well as the quadriceps and hamstrings muscle forces during vertical jump exercise. All these forces are in agreement with data reported in the literature.

Moreover, the descent phase of jumping is compared with the descent phase of regular squat exercise. The comparison shows that the motion of the tibio-femoral contact point on the tibial plateau is in agreement with data reported in the literature.

An advancement in this study would be to investigate the effects of the arm swing, change in landing style, or an improvement in the model. Improvement of this model may include more refined model of finding the tibiofemoral center of rotation, more refined model of patello-femoral contact force calculation, anatomical refinement, to include several fibers for each ligament behavior, and articular cartilage properties to allow for deformable contact.

5.4 Limitations. The present model is not entirely an anatomical description of the human knee. The femoral condyle is modeled as two circles approximating the tibio-femoral and patello-femoral condylar contact arcs, and the tibial plateau is modeled as a straight line, as shown in Fig. 3. The present model is a 2D model. Therefore, medial and lateral contact forces cannot be assessed, and internal-external rotation cannot be captured. Moreover, 2D models approximate muscle forces by their projections on the sagittal plane. The contact point, which is related to the tibiofemoral center of rotation, is properly captured. The trans-epicondylar motion is properly captured through the marker-based approach, but not the geometric center axis described in Refs. [30–31]. The geometric center would better represent the tibiofemoral center of rotation. Therefore, although the insertion points were anatomical, the magnitude of PCL force was calculated through an optimization process. Another limitation of this work is that only one set of experimental data is presented, and therefore, there is no comparison between multiple sets of data of the

exercise. Also, this work does not investigate the effect of maximum knee flexion angle of jumping on the exercise performance and/or internal forces' magnitudes. The maximum knee flexion angle in this research is approximately 95 deg. Cases of deep knee flexion [56] of jumping were not considered here.

Funding Data

- National Science Foundation CBET Division (Grant No. #1126763; Funder ID: 10.13039/100000001).

References

- [1] Nishida, I., Maeda, M., Gordon, D., Robertson, E., and Shirase, K., 2011, "Development of an Ergonomic Musculoskeletal Model to Estimate Muscle Forces During Vertical Jumping," *Procedia Eng.*, **13**, pp. 338–343.
- [2] Babic, J., and Lenarcic, J., 2007, "Vertical Jump: Biomechanical Analysis and Simulation Study," *Humanoid Robots: New Developments*, I-Tech, Vienna, Austria, pp. 551–564.
- [3] Bobbert, M. F., Jaspers, R. T., and Sijpkens, I. W. T., 2007, "Muscle Activation Patterns in Squat Jumps From Different Initial Positions," *J. Biomech.*, **40**(2), p. S300.
- [4] Winter, D. A., 1995, "Human Balance and Posture Control During Standing and Walking," *Gait Posture*, **3**(4), pp. 193–214.
- [5] Cleather, D. J., Goodwin, J. E., and Bull, A. M. J., 2013, "Hip and Knee Joint Loading During Vertical Jumping and Push Jerking," *Clin. Biomech.*, **28**(1), pp. 98–103.
- [6] Samozino, P., Morin, J.-B., Hintzy, F., and Belli, A., 2008, "A Simple Method for Measuring Force, Velocity and Power Output During Squat Jump," *J. Biomech.*, **41**(14), pp. 2940–2945.
- [7] Spägle, T., Kistner, A., and Gollhofer, A., 1999, "A Multi-Phase Optimal Control Technique for the Simulation of a Human Vertical Jump," *J. Biomech.*, **32**(1), pp. 87–91.
- [8] Pflum, M. A., Shelburne, K. B., Torry, M. R., Decker, M. J., and Pandey, M. G., 2004, "Model Prediction of Anterior Cruciate Ligament Force During Drop-Landings," *Med. Sci. Sports Exerc.*, **36**(11), pp. 1949–1958.
- [9] Dufek, J. S., and Bates, B. T., 1991, "Biomechanical Factors Associated With Injury During Landing in Jump Sports," *Sports Med.*, **12**(5), pp. 326–337.
- [10] Prihutsky, B. I., and Zatsiorsky, V. M., 1994, "Tendon Action of Two-Joint Muscles: Transfer of Mechanical Energy Between Joints During Jumping, Landing, and Running," *J. Biomech.*, **27**(1), pp. 25–34.
- [11] Bates, N. A., Ford, K. R., Myer, G. D., and Hewett, T. E., 2013, "Impact Differences in Ground Reaction Force and Center of Mass Between the First and Second Landing Phases of a Drop Vertical Jump and Their Implications for Injury Risk Assessment," *J. Biomech.*, **46**(7), pp. 1237–1241.
- [12] Norcross, M. F., Lewek, M. D., Padua, D. A., Shultz, S. H., Weinhold, P. S., and Blackburn, J. T., 2013, "Lower Extremity Energy Absorption and Biomechanics During Landing—Part I: Sagittal-Plane Energy Absorption Analyses," *J. Athletic Train.*, **48**(6), pp. 748–756.
- [13] Pappas, E., Hagins, M., Sheikhzadeh, A., Nordin, M., and Rose, D., 2007, "Biomechanical Differences Between Unilateral and Bilateral Landings From a Jump: Gender Differences," *Clin. J. Sport Med.*, **17**(4), pp. 263–268.
- [14] Schellenberg, F., Oberhofer, K., Taylor, W. R., and Lorenzetti, S., 2015, "Review of Modelling Techniques for In Vivo Muscle Force Estimation in the Lower Extremities During Strength Training," *Comput. Math. Methods Med.*, **2015**, p. 1.
- [15] Hirayama, K., 2014, "Acute Effects of an Ascending Intensity Squat Protocol on Vertical Jump Performance," *J. Strength Cond. Res.*, **28**(5), pp. 1284–1288.
- [16] Pérez-Castilla, A., McMahon, J. J., Comfort, P., and García-Ramos, A., 2017, "Assessment of Loaded Squat Jump Height With a Free-Weight Barbell and Smith Machine: Comparison of the Take-Off Velocity and Flight Time Procedures," *J. Strength Cond. Res.*, **32**(6), pp. 38–41.
- [17] Fukutani, A., Takei, S., Hirata, K., Miyamoto, N., Kanehisa, H., and Kawakami, Y., 2014, "Influence of the Intensity of Squat Exercises on the Subsequent Jump Performance," *J. Strength Cond. Res.*, **28**(8), pp. 2236–2243.
- [18] Paul, J., and Kumar, S., 2018, "Comparative Effect of Squat Jump and Split Jump Exercise on Dynamic Balance Among Female Netball Players," *Int. J. Physiother.*, **5**(2), pp. 57–62.
- [19] Blajer, W., Dziewiecki, K., and Mazur, Z., 2007, "Multibody Modeling of Human Body for the Inverse Dynamics Analysis of Sagittal Plane Movements," *Multibody Syst. Dyn.*, **18**(2), pp. 217–232.
- [20] Kim, Y.-K., and Kim, Y. H., 2011, "Intersegmental Dynamics of the Lower Limb in Vertical Jumps," *J. Mech. Sci. Technol.*, **25**(7), pp. 1817–1822.
- [21] Caruntu, D. I., and Hefzy, M. S., 2004, "3-D Anatomically Based Dynamic Modeling of the Human Knee to Include Tibio-Femoral and Patello-Femoral Joints," *ASME J. Biomech. Eng.*, **126**(1), pp. 44–53.
- [22] Hamai, S., Dunbar, N. J., Moro-oka, T., Miura, H., Iwamoto, Y., and Banks, S. A., 2013, "Physiological Sagittal Plane Patellar Kinematics During Dynamic Deep Knee Flexion," *Int. Orthop. (SICOT)*, **37**(8), pp. 1477–1482.
- [23] von Eisenhart-Rothe, R., Siebert, M., Bringmann, C., Vogl, T., Englmeier, K.-H., and Graichen, H., 2004, "A New In Vivo Technique for Determination of

- 3D Kinematics and Contact Areas of the Patello-Femoral and Tibio-Femoral Joint," *J. Biomech.*, **37** (6), pp. 927–934.
- [24] DeFrate, L. E., Nha, K. W., Papannagari, R., Moses, J. M., Gill, T. J., and Li, G., 2007, "The Biomechanical Function of the Patellar Tendon During in-Vivo Weight-Bearing Flexion," *J. Biomech.*, **40**(8), pp. 1716–1722.
- [25] Varadarajan, K. M., Gill, T. J., Freiberg, A. A., Rubash, H. E., and Li, G., 2010, "Patellar Tendon Orientation and Patellar Tracking in Male and Female Knees," *J. Orthop. Res.*, **28**(3), pp. 322–328.
- [26] Yue, B., Varadarajan, K. M., Ai, S., Tang, T., Rubash, H. E., and Li, G., 2011, "Differences of Knee Anthropometry Between Chinese and White Men and Women," *J. Arthroplasty*, **26**(1), pp. 124–130.
- [27] Granados, E., 2015, "Two-Dimensional Dynamics Model of the Lower Limb to Include Viscoelastic Knee Ligaments," MS thesis, The University of Texas, Pan American, Edinburg, TX.
- [28] Hill, P. F., Vedi, V., Williams, A., Iwaki, H., Pinskerova, V., and Freeman, M. A. R., 2000, "Tibiofemoral Movement 2: The Loaded and Unloaded Living Knee Studied by MRI," *Bone Jt. J.*, **82**(8), pp. 1196–1198.
- [29] Shelburne, K. B., and Pandey, M. G., 1998, "Determinants of Cruciate-Ligament Loading During Rehabilitation Exercise," *Clin. Biomech.*, **13**(6), pp. 403–413.
- [30] Most, E., Axe, J., Rubash, H., and Li, G., 2004, "Sensitivity of the Knee Joint Kinematics Calculation to Selection of Flexion Axes," *J. Biomech.*, **37**(11), pp. 1743–1748.
- [31] Kozanek, M., Hosseini, A., Liu, F., Van de Velde, S. K., Gill, T. J., Rubash, H. E., and Li, G., 2009, "Tibiofemoral Kinematics and Condylar Motion During the Stance Phase of Gait," *J. Biomech.*, **42**(12), pp. 1877–1884.
- [32] Bolsterlee, B., Gandevia, S. C., and Herbert, R. D., 2016, "Ultrasound Imaging of the Human Medial Gastrocnemius Muscle: How to Orient the Transducer so That Muscle Fascicles Lie in the Image Plane," *J. Biomech.*, **49**(7), pp. 1002–1008.
- [33] Yoshioka, Y., Siu, D. W., Scudamore, R. A., Derek, T., and Cooke, V., 1989, "Tibial Anatomy and Functional Axes," *J. Orthop. Res.*, **7**(1), pp. 132–137.
- [34] Mow, V. C., Ateshian, G. A., and Spilker, R. L., 1993, "Biomechanics of Diarthrodial Joints: A Review of Twenty Years of Progress," *ASME J. Biomech. Eng.*, **115**(4B), pp. 460–467.
- [35] Flandry, F., and Hommel, G., 2011, "Normal Anatomy and Biomechanics of the Knee," *Sports Med. Arthroscopy Rev.*, **19**(2), pp. 82–92.
- [36] Bartel, D. L., Davy, D. T., and Keaveny, T. M., 2006, *Orthopaedic Biomechanics*, Pearson/Prentice Hall, Upper Saddle River, NJ.
- [37] Cleather, D., and Bull, A. M. J., 2010, "Influence of Inverse Dynamics Methods on the Calculation of Inter-Segmental Moments in Vertical Jumping and Weightlifting," *BioMed. Eng. Online*, **9**(1), p. 74.
- [38] Seireg, A., and Arvikar, R. J., 1973, "A Mathematical Model for Evaluation of Forces in Lower Extremities of the Musculo-Skeletal System," *J. Biomech.*, **6**(3), pp. 313–326.
- [39] Moissenet, L., Chèze, L., and Dumas, R., 2014, "A 3D Lower Limb Musculo-skeletal Model for Simultaneous Estimation of Musculo-Tendon, Joint Contact, Ligament and Bone Forces During Gait," *J. Biomech.*, **47**(1), pp. 50–58.
- [40] Lin, Y.-C., Walter, J. P., Banks, S. A., Pandey, M. G., and Fregly, B. J., 2010, "Simultaneous Prediction of Muscle and Contact Forces in the Knee During Gait," *J. Biomech.*, **43**(5), pp. 945–952.
- [41] Seireg, A., and Arvikar, R. J., 1975, "The Prediction of Muscular Load Sharing and Joint Forces in the Lower Extremities During Walking," *J. Biomech.*, **8**(2), pp. 89–102.
- [42] Czaplicki, A., Silva, M., Ambrósio, J., Jesus, O., and Abrantes, J., 2006, "Estimation of the Muscle Force Distribution in Ballistic Motion Based on a Multi-body Methodology," *Comput. Methods Biomech. Biomed. Eng.*, **9**(1), pp. 45–54.
- [43] Crowninshield, R. D., and Brand, R. A., 1981, "A Physiologically Based Criterion of Muscle Force Prediction in Locomotion," *J. Biomech.*, **14**(11), pp. 793–801.
- [44] Pierce, J. E., and Li, G., 2005, "Muscle Forces Predicted Using Optimization Methods Are Coordinate System Dependent," *J. Biomech.*, **38**(4), pp. 695–802.
- [45] Anderson, F. C., and Pandey, M. G., 2001, "Static and Dynamic Optimization Solutions for Gait Are Practically Equivalent," *J. Biomech.*, **34**(2), pp. 153–161.
- [46] Nigg, B. M., and Herzog, W., 2007, *Biomechanics of the Musculo-Skeletal System*, 3rd ed., Wiley, Hoboken, NJ.
- [47] Winter, D. A., 2009, *Biomechanics and Motor Control of Human Movement*, Wiley, Hoboken, NJ.
- [48] De Leva, P., 1996, "Adjustments to Zatsiorsky-Seluyanov's Segment Inertia Parameters," *J. Biomech.*, **29**(9), pp. 1223–1230.
- [49] Zatsiorsky, V. M., Seluyanov, V. N., and Chugunova, L. G., 1990, "Methods of Determining Mass-Inertial Characteristics of Human Body Segments," *Contemporary Problems of Biomechanics*, G. G. Chemyi, and S. A. Regirer, eds., CRC Press, Boca Raton, FL, pp. 272–291.
- [50] Yu, B., Gabriel, D., Noble, L., and An, K.-N., 1999, "An, K.-N., Estimate of the Optimum Cutoff Frequency for the Butterworth Low-Pass Digital Filter," *J. Appl. Biomech.*, **15**(3), pp. 318–329.
- [51] Weiss, L. W., Ferreira, L. C., Feldman, C. R., Schilling, B. K., and Hammond, K. G., 2011, "Association of Accelerometer-Derived Jump Squat Power With Drop Vertical Jump Displacement," *J. Strength Cond. Res.*, **25**, pp. S15–S16.
- [52] Bisseling, R. W., and Hof, A. L., 2006, "Handling of Impact Forces in Inverse Dynamics," *J. Biomech.*, **39**(13), pp. 2438–2444.
- [53] Slater, L. V., and Hart, J. M., 2017, "Muscle Activation Patterns During Different Squat Techniques," *J. Strength Cond. Res.*, **31**(3), pp. 667–676.
- [54] Murakami, K., Hamai, S., Okazaki, K., Ikebe, S., Shimoto, T., Hara, D., Mizuchi, H., Higaki, H., and Iwamoto, Y., 2016, "In Vivo Kinematics of Healthy Male Knees During Squat and Golf Swing Using Image-Matching Techniques," *Knee*, **23**(2), pp. 221–226.
- [55] Van Hooren, B., and Zolotarjova, J., 2017, "The Difference Between Countermovement and Squat Jump Performances: A Review of Underlying Mechanisms With Practical Applications," *J. Strength Cond. Res.*, **31**(7), pp. 2011–2020.
- [56] Caruntu, D. I., Hefzy, M. S., Goel, V. K., Goitz, H. T., Dennis, M. J., and Agrawal, V., 2003, "Modeling the Knee Joint in Deep Flexion: 'Thigh and Calf' Contact," *Summer Bioengineering Conference*, Key Biscayne, FL, June 25–29, pp. 459–460.